AD-A106 419 AIR FORCE GEOPHYSICS LAB HANSCOM AFB MA F/G 4/1
THE CONVERSION OF AIRCRAFT ICE CRYSTAL MEASUREMENTS INTO TERMS --ETC(U)
JUN 81 R O BERTHEL

UNCLASSIFIED AFGL-TR-81-0173 NL

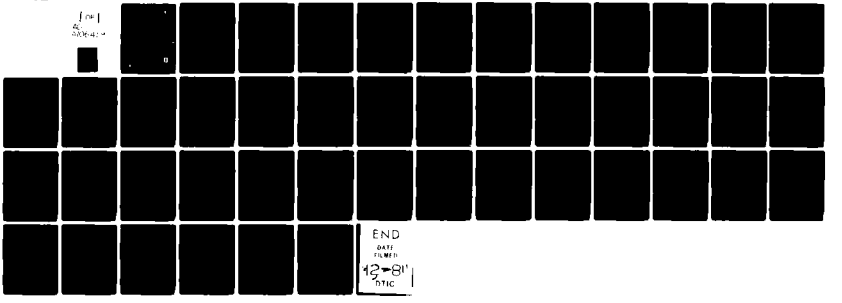

END
DATE FILMED
12-81
DTIC

LEVEL II

(12)

(14) AFGL-TR-81-0173, AFGL-ERP-745

ENVIRONMENTAL RESEARCH PAPERS, NO. 745

AD A106419

(6) The Conversion of Aircraft Ice Crystal Measurements Into Terms of Liquid Water Using Simulated Data.

ROBERT G. BERTHEL

(10)

(11) 16 Jun 1981

(12) 46

(16) 6670, 2310

(17) 12, 65

METEOROLOGY DIVISION PROJECT 6670, 2310

AIR FORCE GEOPHYSICS LABORATORY

HANSCOM AFB, MASSACHUSETTS 01731

AIR FORCE SYSTEMS COMMAND, USAF

This report has been reviewed by the ESD Information Office (OI) and is releasable to the National Technical Information Service (NTIS).

This technical report has been reviewed and is approved for publication.

FOR THE COMMANDER

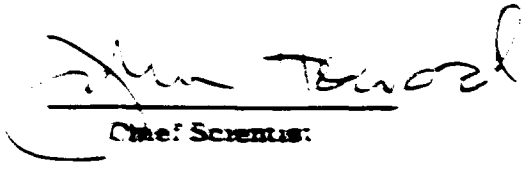

Chief Scientist

Qualified requestors may obtain additional copies from the Defense Technical Information Center. All others should apply to the National Technical Information Service.

Unclassified
SECURITY CLASSIFICATION OF THIS PAGE (When Data Entered)

REPORT DOCUMENTATION PAGE	READ INSTRUCTIONS BEFORE COMPLETING FORM
1. REPORT NUMBER: AFGL-TR-81-0173	2. GOVT ACCESSION NO.: AD-A106 429
3. RECIPIENT'S CATALOG NUMBER:	
4. TITLE (and Subtitle): THE CONVERSION OF AIRCRAFT ICE CRYSTAL MEASUREMENTS INTO TERMS OF LIQUID WATER USING SIMULATED DATA	5. TYPE OF REPORT & PERIOD COVERED: Scientific. Interim.
	6. PERFORMING ORG. REPORT NUMBER: ERP No. 745
7. AUTHOR(s): Robert O. Berthel	8. CONTRACT OR GRANT NUMBER(s):
9. PERFORMING ORGANIZATION NAME AND ADDRESS: Air Force Geophysics Laboratory (LYC) Hanscom AFB Massachusetts 01731	10. PROGRAM ELEMENT, PROJECT, TASK AREA & WORK UNIT NUMBERS: 62101F 61102F 66701201 2310G501
11. CONTROLLING OFFICE NAME AND ADDRESS: Air Force Geophysics Laboratory (LYC) Hanscom AFB Massachusetts 01731	12. REPORT DATE: 16 June 1981
	13. NUMBER OF PAGES: 46
14. MONITORING AGENCY NAME & ADDRESS (if different from Controlling Office):	15. SECURITY CLASS. (of this report): Unclassified
	15a. DECLASSIFICATION DOWNGRADING SCHEDULE:

16. DISTRIBUTION STATEMENT (of this Report)

Approved for public release; distribution unlimited.

17. DISTRIBUTION STATEMENT (of the abstract entered in Block 20, if different from Report)

18. SUPPLEMENTARY NOTES

19. KEY WORDS (Continue on reverse side if necessary and identify by block number)

Ice crystal	Bullets
L to d conversion	Plates
Aircraft measurements	Cloud physics
Columns	Liquid water content
Needles	

20. ABSTRACT (Continue on reverse side if necessary and identify by block number)

This investigation presents simulated environments of ice crystals to computer analysis as a means of imitating particle measurements made by electro-optical devices such as the Particle Measuring System's 1-D instrument. A mathematical model is developed so that single crystals of known geometric form can be processed by considering each crystal's spatial relationship to the assumed measuring instrument. Crystal orientation is defined using a random number technique. The results of the assumed

DD FORM 1 JAN 73 1473

Unclassified
SECURITY CLASSIFICATION OF THIS PAGE (When Data Entered)

20. Abstract (Continued)

measurements are converted into mass of equivalent liquid water by different methods and are compared with the known mass of the simulated environment.

Relationships are derived for the conversion of several forms of single ice crystals into terms of equivalent melted diameters of liquid water and a comparison is made between the mass calculated from the derived equations with the conversion equations relating measured length to equivalent melted diameter currently in use.

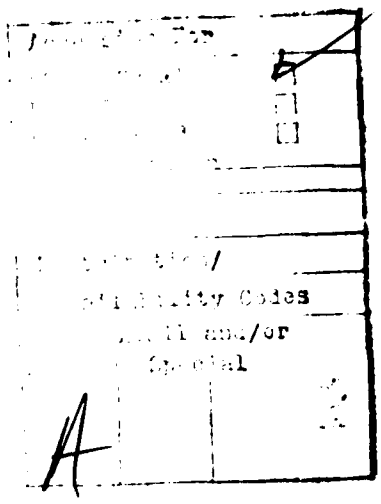

Contents

Illustrations

Tables

Tables

The Conversion of Aircraft Ice Crystal Measurements Into Terms of Liquid Water Using Simulated Data

1. INTRODUCTION

The determination of the water content, or mass, of clouds and/or precipitation has dominated the efforts of many meteorological groups for a number of years. As part of their mission objectives in programs concerned with weather erosion,[1-4] large scale cloud systems,[5,6] and cirrus studies[7-13] the Cloud Physics Branch of the Air Force Geophysics Laboratory (AFGL), for example, has been determining the mass of many diverse types of hydrometeors from the particle spectra measured with an instrumented MC-130E aircraft.

The absence of the means to measure the water content of hydrometeors directly and reliably necessitates the measuring of the particle spectra and calculating mass through knowledge of particle size and number concentration. In past years, much time-consuming labor has been expended in the analysis of aircraft-acquired particle spectra from instruments such as the aluminum foil sampler[14,15] and the airborne continuous particle replicator[16,17] in an attempt to define spectra for the determination of mass. With the relatively recent operational use of specialized electrooptical instrumentation, such as the Particle Measuring System's (PMS) one-dimensional instrument (1-D), hydrometeor spector can now be conveniently measured

(Received for publication 15 June 1981)

Because of the large number of references cited above, they will not be listed here. See References, page 43.

and efficiently processed with computers.[18] Assuming an errorless operation of such an instrument, accurate determinations of mass, within the bounds of some inherent variability, are now possible. This is particularly true in rain situations when the measured hydrometeors can be considered spherical water drops. Ice particles present a more complex problem, however, since knowledge of geometric form and dimensions are required for the calculation of volume and an assumed density is needed to convert the ice volume to an equivalent mass of liquid water.

The investigation presented in this report is basically concerned with aircraft measurements of single ice crystals and the subsequent determination of mass. It is a study of hypothetical experimental situations where simulated ice crystals of known dimensions and densities are "measured" by an equally simulated electro-optical aircraft instrument, of the PMS 1-D type, where the shadows from particles passing through a laser beam occlude diodes in a sensing array and are electronically counted and classified as to size. All the simulations are conducted with a computer programmed mathematical model where mass is calculated from the assumed geometry and spectra of pristine crystals of specific type, aggregates not included.

2. MODEL DEVELOPMENT

The first crystal considered was a solid, cylindrical ice column with a specified length to diameter ratio. A cylindrical structure was used in the development of the model because of the relative ease of visualizing this form in the following discussion. Conversion to the natural hexagonal structure is undertaken later in Section 6.

The mass (m) of such configuration is

$$m = \rho_I \pi D^2 \, L/4 \quad (g), \tag{1}$$

where the diameter (D) and length (L) of the column are in millimeters and ρ_I (g mm^{-3}) is the density of ice.

When the diameter is expressed in terms of length as

$$D = L/X \quad (mm) \tag{2}$$

---

18. Knollenberg, R.G. (1970) The optical array: an alternative to scattering or extinction for airborne particle size determination, J. Appl. Meteor. 1:86-103.

Eq. (1) then becomes

$$m = \rho_I \pi L^3/4 X^2 \quad (g) . \tag{3}$$

(The use of a linear relationship of D with L shows a general agreement with the experimental results of other investigations. A discussion of the geometric relationships used in this study and those derived from experimental data is included in Section 7.)

It is convenient in cloud physics work to express the mass of any hydrometeor in terms of the equivalent mass of liquid water (M) contained in a spherical water drop as

$$M = \rho_\omega \pi d^3/6 \quad (g) , \tag{4}$$

where d is the diameter in millimeters of the spherical drop and ρ_ω (g mm^{-3}) is the density of water. The equivalent melted diameter (d_e) of a spherical drop resulting from the melting of a cylindrical columnar ice crystal is found by equating Eqs. (3) and (4) as

$$\rho_\omega \pi d_e^3/6 = \rho_I \pi L^3/4X^2 \tag{5}$$

and solving for d_e as

$$d_e = \left(\frac{\rho_I 6 L^3}{\rho_\omega 4X^2} \right)^{1/3} \quad (mm) . \tag{6}$$

When ρ_ω = 0.001 g mm^{-3} and ρ_I is considered to be 0.0009 g mm^{-3}, Eq. (6) becomes

$$d_e = (1.35/X^2)^{1/3} L \quad (mm). \tag{7}$$

In the first situation considered, the diameter of the ice column was defined to be 1/4 the length and thus, for this particular case where X = 4,

$$d_e = 0.4386 L \quad (mm) . \tag{8}$$

The equivalent mass of liquid water contained in one m^3 from one such crystal can be determined by substituting the d_e of Eq. (8) for the d of Eq. (4) as

$$M = \frac{\rho_\omega \pi}{6} (0.4386\ L)^3 \qquad (g\ m^{-3}) . \tag{9}$$

The total mass from a number (n) of this type crystal is found by summing the individual M's as

$$M = M_1 + M_2 + M_3 \ldots + M_n \qquad (g\ m^{-3}) . \tag{10}$$

The radar reflectivity (Z) from one m^3 containing a crystal is defined as being equal to the sixth power of the diameter of the assumed spherical water drop as

$$Z = (0.4386\ L)^6 \qquad (mm^6\ m^{-3}) \tag{11}$$

and the total reflectivity from a number of these specified columns can be expressed as

$$Z = Z_1 + Z_2 + Z_3 \ldots + Z_n \qquad (mm^6\ m^{-3}) . \tag{12}$$

When a specified environment of n cylindrical ice columns is considered, the M and Z can be determined by applying the crystal lengths to Eqs. (9) and (10) for M and Eqs. (11) and (12) for Z. If these same hydrometeors are assumed to be measured with an airborne instrument, the resulting L's will be classified in discrete size classes and M and Z are then determined by

$$M = \rho_\omega \pi/6 \sum_{i=1}^{i=n} d_{e_i}^3 \ N_i \qquad (g\ m^{-3}) \tag{13}$$

and

$$Z = \sum_{i=1}^{i=n} d_{e_i}^6 \ N_i \qquad (mm^6\ m^{-3}) \tag{14}$$

where N_i is the number of particles per m^3 in class "i" and d_{e_i} is the mid-equivalent melted diameter of that class which is found by applying the midclass L to Eq. (8). If the spatial positioning of these columns were such that the true geometric lengths were measured, then the calculated M and Z would be the true values of that distribution. However, this condition specifies that each individual column has to pass through the measuring instrument's field of view with its longitudinal axis precisely aligned with the diode array to insure a true measure of length. This situation would require a field of freely falling ice columns, preferentially oriented parallel to each other in the horizontal plane which, although not impossible, is highly improbable.

In the absence of a force field, which could serve to align the crystals in a preferred manner, such as an electric charge field,[19] one must assume that freely falling crystals would present a random selection of all probable orientations in the horizontal. Figure 1 is a diagramatic view looking down upon such a column and shows the possible angles of orientation that could be presented to the measuring instrument.

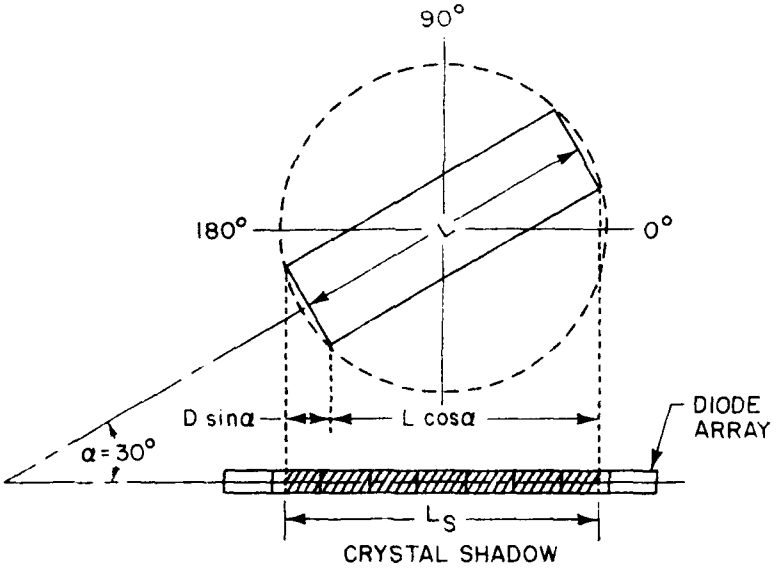

Figure 1. The Shadow Produced by a Columnar Crystal with a 30° Orientation from the Axis of the Diode Array as it Passes Through the Measuring Instrument

19. Crane, R.K. (1978) Evaluation of Uncertainties in the Estimation of Hydrometeors Mass Concentrations using Spandar Data and Aircraft Measurements, Scientific Report No. 1, AFGL-TR-78-0118, AD A059 223, 107 pp.

It is apparent that any angle in the 360° dashed circle, circumscribed by a column rotating in the horizontal plane, is possible but, since the angles in each quadrant present identical configurations, there is quadrant symmetry and only the angles of 0 through 90° have to be considered. It is evident that an angle of 0° (parallel with the diode array) would result in the true length of the crystal being shadowed on the sensing diodes whereas an angle of 90° would give a shadow equal to the column's diameter. Angles between these extremes can present shadows ranging in size from the crystal diameter up to slightly larger than the geometric crystal length. The spatial positioning of a freely falling crystal and consequently, the crystal's angle of orientation with the measuring diode array, is a chance effect and can be simulated by use of a nonbiased selection technique such as the association of a random number with a random angle.

The dotted lines in Figure 1 indicate the shadow length that would be produced by a column when its axis is orientated 30° from the axis of the diode array. The length of shadow (L_S) cast by this column as it moves through the beam of light at an angle of α degrees can be defined as

$$L_S = L \cos \alpha + D \sin \alpha \qquad \text{(mm)} . \tag{15}$$

It is the second term of this equation or the shadow component attributed to the ends of this cylindrical crystal that can cause L_S values in excess of actual L. This is demonstrated in Figure 2 where the shadow length of a 1 mm column is plotted from 0 to 90° as the solid line along with the component parts of Eq. (15) namely, the contribution from the length (L Cos α) as the dotted line and that from the crystal diameter (D Sin α) as the dashed line. (It must be pointed out that the PMS 1-D instrument has a shadow density threshold on each diode and will not respond to insufficient occlusion. This would act to minimize or negate this "excess length effect." No adjustment has been made in this study to compensate for this effect since this investigation is of a theoretical nature.)

A second degree of freedom in the orientation of the crystals is possible, this being in the vertical plane perpendicular to the level flight plane of the sampling aircraft. It is generally accepted that a columnar crystal will fall so that its axis is somewhat parallel to the wings of a level flying aircraft. The freedom in this case was assumed to be ±0 to 45° relative to the horizontal. The reason behind this decision is that the turbulent wind shear, normally experienced during actual experimental conditions, would have an effect on the crystals' spatial positioning. As an aircraft passes through a field of ice crystals it would encounter groups of particles that are experiencing varying amounts of shear. Therefore, the distance traveled by an aircraft in a sampling time period would expose the measuring device to crystals that are tilted at various degrees in the vertical plane. It is

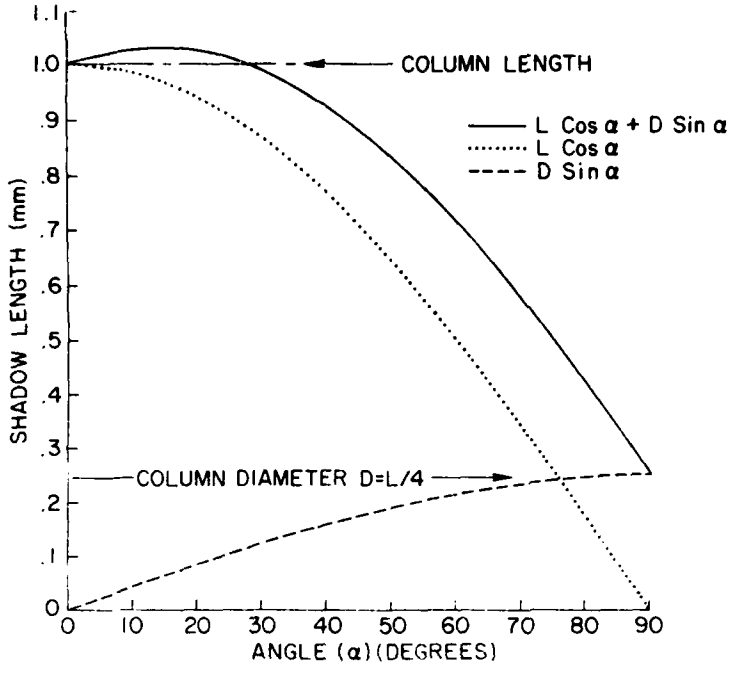

Figure 2. The Shadow Lengths (L_S) Produced by a 1 mm Columnar Crystal with a Diameter of 0.025 mm (Solid Line) at Angles of 0 to 90° with the Diode Array

assumed that a random degree of tilt in the vertical would simulate this turbulent wind shear effect. Angles in this plane that are larger than 45° would most likely represent crystals that are experiencing severe turbulent conditions and tumbling, which is not envisioned as being the typical or usual situation. (Different atmospheric effects can alter crystal spatial positioning depending upon crystal size and/or shape. No consideration has been made for these possible variations in this study and the assumptions of random positioning, as described above, have been applied to all crystal types and sizes.)

The shadow length (L_S) obtained from the two degrees of freedom in a column's orientation can be expressed as

$$L_{SH} = L \text{ Cos } \alpha_H + D \text{ Sin } \alpha_H \tag{16}$$

and

$$L_S = L_{SH} \text{ Cos } \alpha_V + D \text{ Sin } \alpha_V \, , \tag{17}$$

where L_{SH} is the shadow length from the orientation of the column at a random angle of 0 to 90° (α_H) in the horizontal plane and α_V is the random angle of 0 to 45° in the vertical plane.

A Tektronix 4052 computer was used to define simulated ice-column environments of known distributions of specified size and number concentrations. The random number generator of the TEK 4052 allowed each individual crystal to be assigned a random angle in both the horizontal and vertical planes. The simulated measuring was accomplished by calculating the shadows that would have been produced had the crystals passed through a light beam. The resulting shadow lengths were then used in Eq. (8) to determine the d_e's which, in turn, were applied to [illegible] (10) for the calculation of M and to Eqs. (11) and (12) for Z. The L_S values [illegible] also classified into 0.025 mm classes and the M and Z, in this case, were determined by calculating the midclass d_e's by using the midclass length values in Eq. (8) and applying them with the corresponding N_i's to Eqs. (13) and (14). Thus, the true M and Z (M_T and Z_T) determined from using the geometric crystal lengths in the equations could be compared with results obtained from simulated experimental conditions.

3. ANALYSIS OF SINGLE-SIZE CYLINDRICAL COLUMNS

The first exercise presented to the computer model was a group of 500 cylindrical columns, all of the exact same size, having lengths of [illegible] mm and diameters of 0.125 mm. The shadow lengths of these columns were calculated using the random orientation process described above. The resulting number density distribution from the classified data is shown in Figure 3.

It is interesting to note that this distribution is heavily biased towards the larger sizes with nearly half (49.2 percent) of the shadow lengths falling within [illegible] percent of the true geometric length of the columns. At first glance, a more even number distribution might be expected since the calculated shadow lengths are the [illegible] result of the crystals' random orientation and the randomly generated angles [illegible] be fairly evenly distributed about a mean value. However, the skewed apportionment of Figure [illegible] repeated [illegible] for [illegible] size [illegible] columns and the [illegible] of the effect [illegible] shown in the plot of [illegible] as a function of [illegible] in Figure 4. The curves of this plot show the shadow lengths that would [illegible] having [illegible] values of 4, [illegible] and [illegible] angles from [illegible] to 90°. The [illegible]-hatched area represents ±10 percent of the [illegible] length [illegible] orientation angles from [illegible] to 45° for this particular [illegible] where [illegible]. It [illegible] that if the randomly generated angles [illegible] equally above and below the mean (±45° in the horizontal [illegible]) [illegible] of the [illegible] values [illegible].

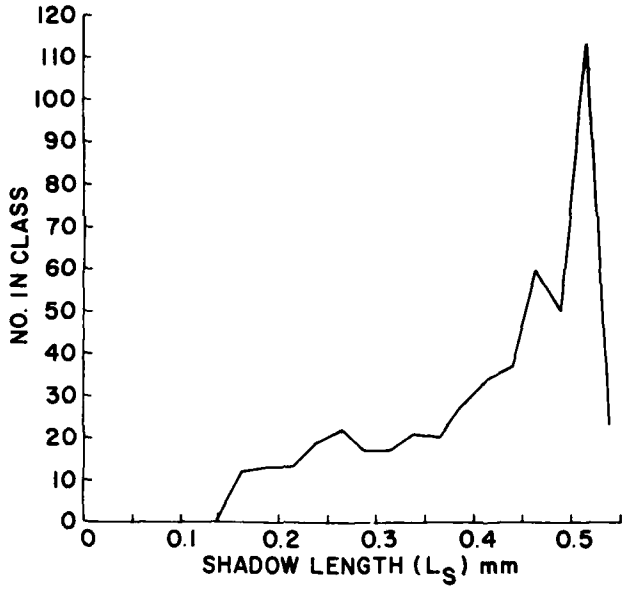

Figure 3. Number Density Distribution of the L_S Values Calculated from the Simulated Environment of 500 Solid Ice Columns of 0.5 mm in Length and 0.0125 mm in Diameter

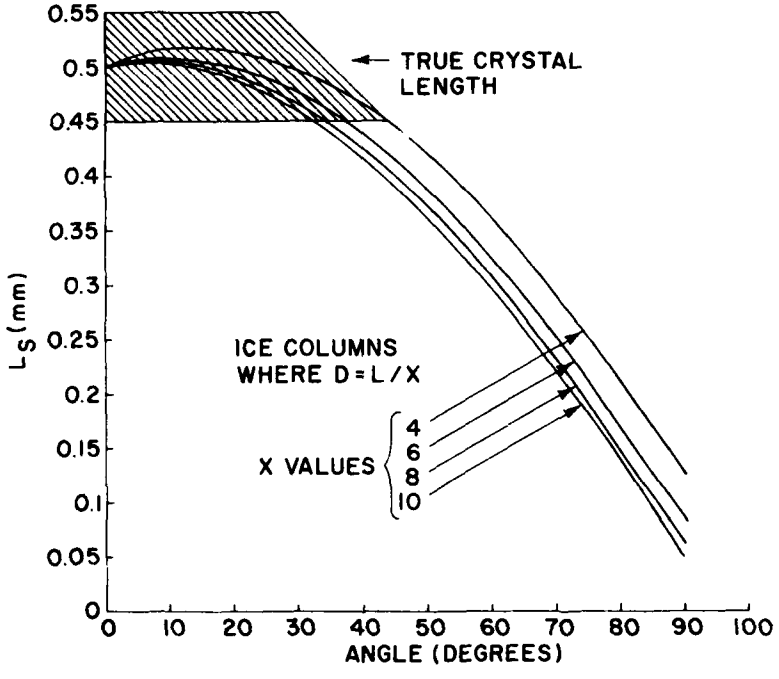

Figure 4. The Shadow Lengths (L_S) Produced by 0.5 mm Columnar Crystals having Diameters of L/4, L/6, L/8 and L/10 mm

fall within 10 percent of the geometric length. The random selection of angles in the vertical plane (a mean of 22.5°) would further amplify this effect and only by having crystal orientation heavily biased toward the larger angles would a more even apportionment become evident.

Line 1 in Table 1 lists the M and Z values that were calculated from the specified physical size of the 500 crystals. Lines 2 through 6 are calculations based on the shadow lengths that resulted from the simulated measurements. Line 2 gives the M and Z values that are calculated if each shadow length is presumed to be a true length. Line 3 shows the results that were obtained from using the classified number density distribution where the M and Z values are the summations calculated from the numbers and mid L_S sizes of each 0.025 mm class. Lines 4, 5 and 6 give the M and Z values that result from using the mean (0.4110 mm), the median (0.4466 mm) and the most frequently occurring value, the mode (0.5125 mm) of the L_S distribution as the length of the columns.

Table 1. The M ($g\ m^{-3}$) and Z ($mm^6\ m^{-3}$) of 500 Cylindrical Columns of 0.5 mm Length Compared to those Calculated from the "Measured" Shadow Lengths

No.	Source	M ($g\ m^{-3}$)	Factor of True M	Z ($mm^6\ m^{-3}$)	Factor of True Z
1	Using L	0.00276	----	0.05562	----
2	Using L_S	0.00182	0.6588	0.03194	0.5743
3	Using Classified Data	0.00182	0.6596	0.03201	0.5756
4	Using Mean	0.00153	0.5552	0.01715	0.3083
5	Using Median	0.00197	0.7128	0.02826	0.5081
6	Using Mode	0.00297	1.0769	0.06450	1.1597

The M and Z calculated from using each individual L_S and the classified L_S data give essentially the same results and indicate that classifying the shadow lengths in 0.025 mm size increments produces little difference. Since the value of the L_S mode is closest to the actual crystal size, it is not surprising that the best agreement with the true M and Z results from the use of this statistical parameter. The calculations from the individual L_S, the L_S classes and the median and mean give M and Z's values much smaller than true.

4. ANALYSIS OF A UNIFORM DISTRIBUTION OF CYLINDRICAL COLUMNS

The next computer simulation was a uniform distribution of cylindrical columns consisting of 10 size groups with 80 particles in each group. The smallest length was 0.05 mm, the largest was 0.5 mm with D = L/4 for all particles and the increment between size groups was 0.05 mm.

The number density distribution of the computed L_S values in 0.025 mm classes is shown in Figure 5. The noticeable change in this plot from Figure 3 is that the large number counts are contained in the low to midsize class range giving the distribution a general negative slope which is an effect that is almost always prevalent in the data obtained from actual aircraft measurements using the PMS 1-D instrument. The difference in the two plots is directly attributable to the spread of the L_S values resulting from the assumed measurements of the randomly oriented columns contained within the different size groups. The plot of the equivalent melted diameters of the columns vs the resulting shadow lengths in Figure 6 show the calculated L_S values that are obtained from each crystal size group and how they overlap those that are produced by other groups. It is apparent that each crystal size group contributes in some degree to the number of smaller L_S sizes. Since the number density distribution of Figure 5 is constructed from the summation of the number of particles within each 0.025 mm class, the smaller size classes result in higher number counts. Also included in Figure 6 are the mean, median, and modal values for both the complete distribution and each column group size.

Table 2 lists the M and Z's and the factors of true M and Z that were calculated using the shadow lengths that resulted from the analysis of the uniform column distribution. The format is the same as that of Table 1.

Once again, the M and Z calculated from using each individual L_S and the classified L_S data are essentially the same. Both have values that are considerably smaller than true. The M and Z's calculated from using the distribution's mean (0.2333 mm), median (0.1950 mm), and modal (0.0375 mm) values are substantially smaller. Calculations were not made using the mean, median, or modal values for each crystal size group since these parameters would be impossible to determine under actual experimental conditions. They are plotted in Figure 6 however, to show the relative changes that occur between the different groups of columns. The results in Table 2 show that the methods that were used in the calculations of M and Z from L_S "measurements" are unable to give good estimates of the true M and Z.

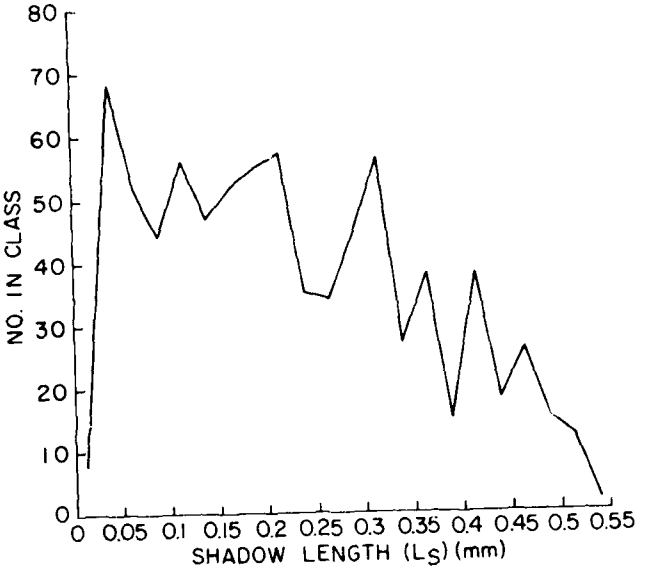

Figure 5. Number Density Distribution of the L_S Values Calculated from the Simulated Environment of 800 Solid Ice Columns in 10 Size Groups of 80 Particles Each

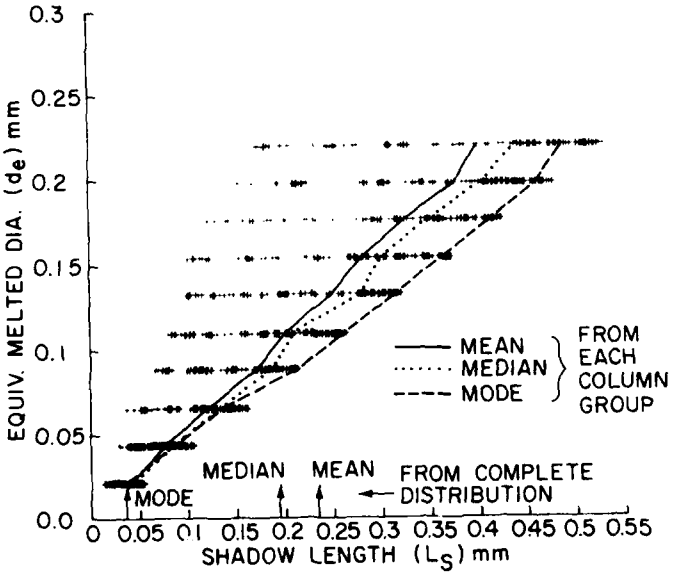

Figure 6. A Plot Showing the Equivalent Melted Diameters of 10 Size Groups of Columns and the Shadow Lengths Calculated from the Simulated Measuring of the 80 Crystals in Each Group

Table 2. The M ($g\ m^{-3}$) and Z ($mm^6\ m^{-3}$) from the Uniform Cylindrical Column Distribution Compared to those Calculated from the "Measured" Shadow Lengths

No.	Source	M ($g\ m^{-3}$)	Factor of True M	Z ($mm^6\ m^{-3}$)	Factor of True Z
1	Using L	0.001340	----	0.01761	----
2	Using L_S	0.000852	0.6374	0.00934	0.5304
3	Using Classified Data	0.000855	0.6399	0.00936	0.5317
4	Using Mean	0.000449	0.3358	0.00892	0.0521
5	Using Median	0.000262	0.1962	0.00313	0.0178
6	Using Mode	2×10^{-6}	0.001395	2×10^{-7}	9×10^{-7}

4.1 Regression Method

When the equivalent melted diameters of the crystals are plotted against their corresponding L_S values in a log-log format, as in Figure 7, the spread attributable to each group of columns tends to become more uniform. This suggests that a regression analysis could be performed on this field of data points to give the line of best fit which could then be used for the conversion of L_S to d_e.

The power function equation of the regression line in Figure 7 is

$$d_e = 0.41151\ L_S^{0.82495} \quad \text{(mm)}. \tag{18}$$

This equation was substituted for the d_e in Eqs. (13) and (14) and calculations were performed to determine the M and Z values using the numbers and classes from the distribution of Figure 5. When these values of M and Z were divided by those derived from the columns' physical sizes, the factor of M/M_T was 0.9249 and Z/Z_T was 0.9393. This shows that when the regression method is used to estimate d_e the subsequent M and Z provides a reasonably close approximation to true (within 8 percent).

4.2 Gamma Method

Another method was developed for estimating the M and Z from the L_S distribution by directly linking Eqs. (13) and (14) to M_T and Z_T.

It was pointed out in Section 3 that the L_S modal peak of the single group of columns was slightly larger than the true length (Figure 3). In the case of the

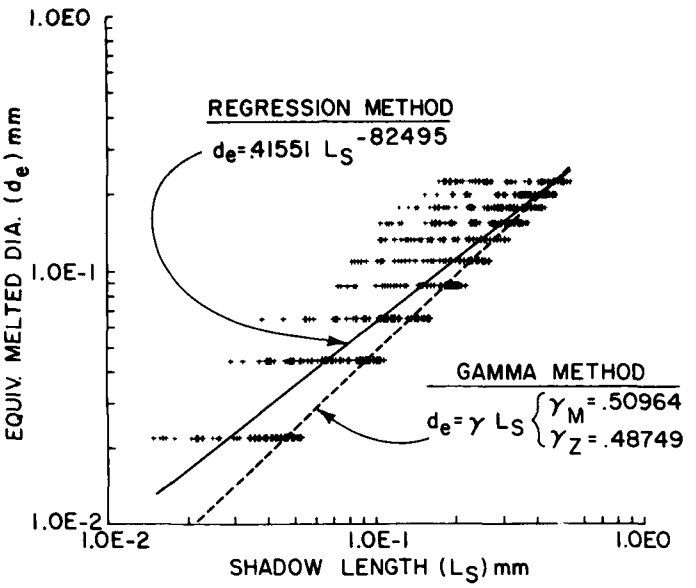

Figure 7. A Logarithmic Plot of the Data in Figure 6 with the "Best Fit" Line from a Regression Analysis and Gamma Method Relationship

uniform distribution, the modal peaks of the 10 size groups fluxuate about the geometric lengths as shown in Figure 6. It is apparent from these plots that the modal values of the measured shadow lengths from randomly orientated crystals of any specific size group will approximate the true geometric lengths.

Also in the case of the uniform distribution, all the columns within the 0.025 to 0.5 mm size range of interest are of the same geometric form and density thus a logarithmic plot of true length vs d_e will give a slope of 1.0. It is assumed in this method, since the modal values approximate the true lengths, that a slope of 1.0 will also be applicable for the randomly orientated crystals. Therefore, the same equation form can be used for the conversion of L_S to d_e for biased conditions where the shadow lengths equal the geometric lengths (Eq. [8]) and also for cases where the shadow lengths are derived from randomly orientated crystals. The difference in the equations will be reflected in the multiplication factor which will be larger in the randomly orientated case to account for the less-than-true length measurements.

Factors relating L_S to d_e can be derived by the following procedure when applied to any designated distribution of crystals for which the M_T and Z_T can be calculated.

When Eq. (18) is written in a general form as

$$d_e = \gamma L_S^{\phi} \qquad (mm), \tag{19}$$

it can be substituted in Eqs. (13) and (14) to give

$$M = \frac{\rho_\omega \pi \gamma^3}{6} \sum_{i=1}^{i=n} L_s^{3\phi} N_i \qquad (g\ m^{-3}) \tag{20}$$

and

$$Z = \gamma^6 \sum_{i=1}^{i=n} L_S^{6\phi} N_i \qquad (mm^{6\ -3}). \tag{21}$$

When M and Z are replaced by M_T and Z_T, and $\phi = 1$, the equations can be solved for γ as

$$\gamma_M = \left(\frac{6\ M_T}{\rho_\omega \pi \sum_{i=1}^{i=n} L_S^3\ N_i} \right)^{1/3} \tag{22}$$

and

$$\gamma_Z = \left(\frac{Z_T}{\sum_{i=1}^{i=n} L_S^6\ N_i} \right)^{1/6} . \tag{23}$$

If Eqs. (22) and (23) are used with a distribution consisting of cylindrical (D = L/4) columns biased in orientation so that $L_S = L$ then both γ_M and γ_Z would equal 0.4386 (Eq. [8]). Since L_S would not normally equal L because of random orientation, then γ_M and γ_Z will be different reflecting the third power size relationship with M and the sixth power with Z.

Thus Eq. (19) where $\phi = 1$, can now be rewritten as

$$d_e = \gamma_M \text{ (or } \gamma_Z) \, L_S \qquad \text{(mm)} \tag{24}$$

and can be used in Eqs. (13) and (14) for the determination of M and Z.

When the M_T and Z_T calculated from the uniform column distribution were substituted in Eqs. (22) and (23), γ_M was 0.50964 and γ_Z was 0.48749. The mid L_S class sizes from the distribution in Figure 6 and the γ_M value were used in Eq. (24) to give a d_e for each class and are plotted in Figure 7. These d_e's and the corresponding class N_i's were used in Eq. (13) for the determination of M. The same procedure was followed using γ_Z in Eq. (24) and then in Eq. (14) for the calculation of Z. The factors of M/M_T and Z/Z_T were 1.0027 and 1.0036. This excellent agreement is not surprising since this method is linked directly to M_T and Z_T, and a very close correspondance between the calculated M and Z from the classified distribution and M_T and Z_T is to be expected.

The method, described in this section will subsequently be referred to as the "gamma" method.

5. COMPARISON OF METHODS

A very important criteria of any method of converting L_S to d_e is its effectiveness in estimating M and Z when applied to all types of particle distributions. One way to establish which method (regression or gamma) will produce the most accurate and least variable M and Z values is to compare the results from both on a number of different simulated crystal environments.

The computer model was changed so that the input numbers of crystals were determined by an exponential distribution function for specified size groups as

$$N_i = N_o \, d^{-\Lambda L} \text{ No. } m^{-3} \, mm^{-1} \tag{25}$$

where N_o is the "zero intercept" of the distribution function in No. m^{-3} mm^{-1} and Λ is the slope of the distribution per mm.

Five column situations were designated each having a different slope of 25, 15, 10, 5, and 0 with 0 being a uniform distribution. The number of size groups, size increments, and maximum crystal lengths were arbitrarily varied so that each situation had a different number total. This procedure resulted in five distinct column distributions with classes exponentially distributed in number content. Thus, each class could be considered as a specific size group of crystals and be

"measured" by the random orientation process previously described. Since each specific size group has an inherent L_S variability because of the assumed random crystal orientation, five separate distributions were analyzed for each situation so that the magnitude of the variance within each set could be established.

The M_T and Z_T were determined for the 25 sets (5 for each situation) and the shadow lengths for each were calculated using Eqs. (16) and (17). A regression analysis was performed on each set of L_S data to determine the coefficient and exponent of the power function equation for the line of best fit as described in Section 4.1. The L_S values were then classified into number density distributions with classes of 0.025 mm. The γ_M and γ_Z values for each set were calculated using the gamma method by substituting M_T and Z_T in Eqs. (22) and (23) with the corresponding class mid-sizes and numbers. Table 3 lists the distribution parameters for the 5 situations and the mean, minimum and maximum values for γ_M, γ_Z and the coefficients and exponents of the regression equations for each of the 25 column distributions.

The largest variation in any of the 4 parameters within each situation was less than 4 percent from the mean values with neither method displaying a distinct advantage. Thus, in the comparison of the results from the five situations, any variations larger than 4 percent from the means will be directly attributable to the differences in the simulated crystal environments.

The means, minimums, and maximums for the same parameters for the combined 25 sets are listed in Table 4.

The variations caused by the physical differences in the assumed column environments are more evident in this table when comparing the variances of γ_M and γ_Z, which were again within 4 percent, to the 11.7 to 17.1 percent of that in the regression equations' coefficients and the -5.7 to 7.1 percent in the exponents.

Since the variations in the coefficients and exponents of power function equations are not necessarily indicative of the variations in the products of the expressions, the M and Z for the L_S distribution of Figure 6 were calculated using the d_e derived from the γ_M, γ_Z and the regression equation for each of the 25 distributions. These results are listed in Table 5 and allow a comparison between the M and Z's calculated from the two methods with the true M and Z's obtained from an independent set of data.

This table shows that a choice of any one of the γ_M's determined from the 25 test distributions can be used in Eq. (24) with the midclass L_S values from Figure 5 to produce d_e's that, in turn, can be substituted into Eq. (13) to give an M that could differ from true by -6.1 to 7.9 percent. A choice of one of the regression equations, on the other hand, could give a difference ranging from -53.3 to 0.2 percent.

Table 3. The Distribution Parameters for the Designated Column Environments and the Mean, Minimum, and Maximum Values for γ_M, γ_Z from the Gamma Method and the Coefficients and Exponents of the Regression Equations for Each Situation

Distribution Parameters						Results of 5 Distributions for Each Situation				
Slope	No. of Size Groups	Max L mm	Total No. of Columns	Method		Mean	Min	$\sigma_{\%}$ (-) from Mean	Max	$\sigma_{\%}$ (+) from Mean
25	20	0.2	5177	Gamma	γ_Z	0.48407	0.47845	1.2	0.49585	2.4
					γ_M	0.51034	0.50673	0.7	0.51747	1.4
				Regression	Coef	0.34852	0.34509	1.0	0.35272	1.2
					Exp	0.86869	0.86568	3.5	0.87210	3.9
15	12	0.3	1950	Gamma	γ_Z	0.48774	0.47182	3.3	0.50253	3.0
					γ_M	0.51033	0.49834	2.3	0.52039	2.0
				Regression	Coef	0.34223	0.33436	2.3	0.34957	2.1
					Exp	0.80420	0.79499	1.1	0.81075	0.8
10	10	0.5	2266	Gamma	γ_Z	0.48332	0.47780	1.1	0.49074	1.5
					γ_M	0.50853	0.50621	0.5	0.51177	0.6
				Regression	Coef	0.33433	0.33184	0.7	0.33542	0.3
					Exp	0.82807	0.82565	0.3	0.82983	0.2
5	20	0.5	1666	Gamma	γ_Z	0.48771	0.47999	1.6	0.49304	1.1
					γ_M	0.51226	0.50418	1.6	0.51771	1.1
				Regression	Coef	0.43353	0.41868	3.4	0.43998	1.5
					Exp	0.88689	0.87216	1.7	0.90289	1.8
0	10	0.5	1000	Gamma	γ_Z	0.48814	0.48204	1.2	0.49591	1.6
					γ_M	0.51383	0.50785	1.2	0.52209	1.6
				Regression	Coef	0.42074	0.40744	3.2	0.43372	3.1
					Exp	0.82609	0.80794	2.2	0.84061	1.8

Table 4. The Mean, Minimum, and Maximum Values of γ_M, γ_Z from the Gamma Method and the Coefficient and Exponent of the Regression Equations for the 25 Combined Distributions

Method		Mean	Min	% (-) from Mean	Max	% (+) from Mean
Gamma	γ_M	0.51106	0.49834	2.5	0.52209	2.2
	γ_Z	0.48625	0.47182	3.0	0.50253	3.3
Regression	Coef	0.37587	0.33184	11.7	0.43998	17.1
	Exp	0.84279	0.79499	5.7	0.90289	7.1

Table 5. Comparison of the M and Z's Calculated Using the Distribution in Figure 5 with the γ_M, γ_Z and Regression Equation for Each of the 25 Column Distributions (M_T = 0.001536, Z_T = 0.01761)

	M (g m^{-3}) from Gamma Method (γ_M)		M (g m^{-3}) from Regression Equations	
	M	$\Delta M/M_T$(%)	M	$\Delta M/M_T$(%)
Mean	0.001353	1.3	0.0008901	-33.4
Minimum	0.001254	-6.1	0.0006243	-53.3
Maximum	0.001442	7.9	0.001339	0.2
	Z (mm^6 m^{-3}) from Gamma Method (γ_Z)		Z (mm^6 m^{-3}) from Regression Equations	
	Z	$\Delta Z/Z_T$(%)	Z	$\Delta Z/Z_T$(%)
Mean	0.01744	-0.9	0.009606	-45.5
Minimum	0.01572	-10.7	0.004393	-75.4
Maximum	0.02118	20.3	0.01971	11.9

When reviewing the results in Tables 4 and 5, it is evident that the regression method is dependent upon the number and size of the crystals that are being measured and upon the distribution of these particles. For example, an exponential distribution with a steep slope would have the majority of particles contained in the smaller size classes and relatively few in the larger ones. Therefore, the slope of the regression line of the d_e vs L_S plot would be heavily weighted by the smaller sizes although it is the lesser number of larger particles that contribute most to the M and Z.

The gamma method, on the other hand, displays considerably less variation with changes in the distribution parameters and leads to the conclusion that it is the more stable method and that the average values of γ_M and γ_Z from the 25 sets could be incorporated as standards for the calculation of reasonable values of M and Z from any distribution of ice columns.

These standards, of course, are particular for nonaggregated ice columns having cylindrical configurations with $D = L/4$. Any variation in the crystal's parameters would change the γ values.

The next section shows how this mathematical approach can be adapted to derive the γ values that are applicable to other single crystals. Section 8 summarizes these results.

6. OTHER COLUMNAR FORMS

The process described herein can be adapted for the study of any simulated ice crystal geometric form that may be defined mathematically. Two important changes are required in the analysis. First, a new relationship of d_e with the crystal parameter L has to be formed (Eq. [8] for columns). Second, the shadow lengths resulting from the possible crystal orientations have to be defined in mathematical terms such as Eqs. (16) and (17) for columns.

6.1 Hollow Columns

A slight change in the mathematics used for solid columns allow the simulation of a hollow column environment. If a cylindrical column has a hollow section, which is in the center of the crystal and aligned with the longitudinal axis, then Eq. (3) can be changed to give the mass as

$$m = \rho_I \pi L^3/4\, X^2 - \rho_I \pi L^3/4\, X_1^2 \qquad (g) \tag{26}$$

or

$$m = (\rho_I \pi L^3/4)\,(1/X^2 - 1/X_1^2) \qquad (g)\,. \tag{27}$$

X in this case is the L to D ratio of the crystals outer diameter and X_1 is that of the inner diameter or the hollow portion. If $X = 4$ and X_1 is arbitrarily given the value of 8, then

$$d_e = 0.3985\ L \qquad (mm) \tag{28}$$

and would, as an example, refer to a ice column of 0.5 mm in length and 0.125 mm in diameter with a hollow center section of 0.0625 mm diameter. The ice wall thickness of such a crystal would be 0.03125 mm. (No attempt was made to associate this hollow column example to observed data. It has been given just to demonstrate how this random orientation concept may be applied to hollow crystals.) Equations (16) and (17) were used to define the L_S values since the geometric configuration of the hollow columns is the same as the solid crystals. The mean γ_M of the 25 distribution in this case was 0.46342 and the mean γ_Z was 0.44103. The variance in both the γ values and regression parameters were substantially the same as those from the solid columns with D's of L/4.

Although these mean γ's were determined using the 5 situation format described in Section 5, a simpler procedure may be utilized in some particular cases. This hollow column form is one such example since the geometric configuration of the hollow column is the same as that of the solid case, thus the deviations caused by shape and spatial positioning can be applied to either case. The difference in the two crystals is the missing center section of the hollow column which effects the relative mass. Dividing the mass of the hollow (Eq. [27]) by that of the solid (Eq. [3]) yields a factor of 0.75. This value taken to the 1/3 power gives a factor of 0.9086 in d_e's (Eq. [28]/Eq. [8]). An approximation of the mean γ's for the hollow columns can be made by multiplying this factor times the γ's of the solid form which gives a γ_M of 0.46435 and a γ_Z of 0.44181 as estimated values. These means are 0.2 percent larger than those determined using the longer, more complicated procedure.

6.2 Hexagonal Columns

If the D of a hexagonal column is considered to be the distance between the apex of two sides to the apex of the opposite two sides when viewing the end of the crystal ("a" axis of the basal plane) then the mass can be expressed as

$$m = \rho_I \, 3\sqrt{3} \, D^2 \, L/8 \qquad \text{(g)} . \tag{29}$$

When D = L/X, Eq. (29) becomes

$$m = \rho_I \, 0.6495 \, L^3/X^2 \qquad \text{(g)} . \tag{30}$$

The short method is applicable again in this case (when X = 4) and Eq. (30) divided by Eq. (3) gives a factor of 0.82697 in mass and a factor of 0.93863 in d_e's. The estimated γ_M now becomes 0.47979 and γ_Z, 0.45641.

A very slight discrepancy can result if a hexagonal column is positioned in such a manner that the part of the shadow attributable to the ends of the crystal is caused by the sides as opposed to the diameter. For example, when $\alpha = 30^{o}$, the shadow length from a column having such positioning would be 1.7 percent less than the shadow from a cylindrical crystal. This effect is minor and is neglected in this study.

6.3 Bullets

If a particular bullet configuration[20] is considered as being a hexagonal column with one end having a 60^{o} pyramid and D = L/X then

$$m = (\rho_I \, 0.6495 \, L^3/X^2) \, (1 - 0.5774/X) \qquad (g) . \tag{31}$$

When X = 4 the mass ratio of a solid cylindrical column to the bullet is 0.70758 and the factor in d_e's is 0.89110. This results in an estimated γ_M of 0.45541 and γ_Z of 0.43330.

Once again, as in the case of columns, the discrepancy in the crystal's shadow that is caused by considering a cylindrical rather than a hexagonal structure is neglected. Also, in this case, the effect caused by the pyramid end is neglected.

6.4 Needles

When X is made equal to 10 in Eq. (7), the crystal form becomes elongated and may be considered as a simulated solid needle (Figure 1) where

$$d_e = 0.23811 \, L \qquad (mm) . \tag{32}$$

Using the 5 situation format of Section 5 and determining the L_S values with Eqs. (16) and (17), the mean values from the gamma method were calculated to be 0.31658 for γ_M and 0.29282 for γ_Z. The variances were -2.0 to 4.0 percent in γ_M and -2.5 to 4.4 percent for γ_Z with both showing a slight increase when compared to those from the columns. Both the coefficient and exponent values from the regression method show a still larger spread with the coefficient's range being from -20.1 to 29.3 percent and the exponents from -10.8 to 11.1 percent.

---

20. Magone, C. and Lee, C. W. (1966) Meteorological classification of natural snow crystals, J. of the Faculty of Science, Hokkaido University, Ser. VII (Geophysics) 4:321-335.

6.5 Hollow Needles

Once again the simplified procedure may be used to estimate the mean γ's that would represent hollow needles from the calculations made for the solid needles. If such a crystal had an arbitrarily selected inner diameter of L/14 and the outer diameter remained as L/10, the mass ratio would be 0.48980 and the factor in d_e's, 0.78827. This gives a γ_M of 0.24955 and a γ_Z of 0.23019 and would refer, for example, to a hollow needle 0.5 mm in length with an outer diameter of 0.05 mm, inner diameter of 0.0357 mm, and a wall thickness of 0.00715 mm. (These dimensions are again used only as an example and are not associated with any experimentally observed data.)

6.6 Hexagonal Plates

If the D of a hexagonal plate is defined as in Section 6.2 the mass can be expressed in terms of D as

$$m = \rho_I \, 3\sqrt{3} \, D^2 \, T/8 \qquad (g) , \tag{33}$$

where T is the thickness of the crystal in mm. If T = D/X then

$$d_e = \frac{1.03739 \, D}{X^{1/3}} \qquad (mm) \tag{34}$$

and when X = 25,

$$d_e = 0.35478 \, D \qquad (mm) . \tag{35}$$

Figure 8 shows a hexagonal plate in the horizontal plane at the angle (30^o) that would present the smallest shadow to the sensing array. The 0^o angle, when the distance designated as the diameter is parallel to the array, will again give a shadow that is equal to D. Crystal symmetry dictates that only the angles of 0 to 30^o have to be considered.

The shadow diameter can thus be defined as

$$D_{SH} = D \cos \alpha_H \qquad (mm) \tag{36}$$

and

$$D_S = D_{SH} \cos \alpha_V \qquad (mm) , \tag{37}$$

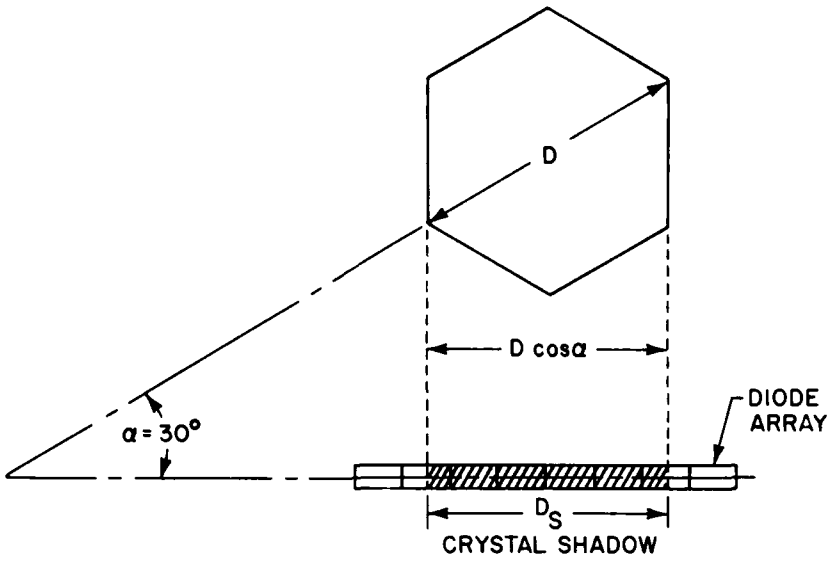

Figure 8. The Shadow Produced by a Hexagonal Plate with a 30° Orientation from the Axis of the Diode Array as it Passes Through the Measuring Instrument

where α_H is a horizontal random angle from 0 to 30° and α_V is, again, a vertical random angle from 0 to 45°. Contributions from the plate's thickness are not taken in consideration in this particular case since the effect is extremely small.

The calculations using the gamma method on the five crystal environment simulations give a mean γ_M of 0.39058 and γ_Z of 0.38528. The variance was -0.6 to 0.7 percent for γ_M and -1.0 to 1.2 percent for γ_Z. The deviation in the parameters of the regression lines were low, being -2.0 to 2.0 in the coefficients and -0.8 to 0.7 in the exponents and the mean exponent of 0.98712 was close to the assumed 1.0 of the gamma method.

6.7 Combined Bullets

A combination of four single bullets, right angles to one another in a common plane and attached at their pyramid ends will form a simple example of a rosette structure. This form would have the shape of a cross with four arms forming 90° angles. The mass of such configuration will be four times that of a single bullet or

$$m = 4\,(\rho_I\, 0.6495\, L_o^3/X^2)\,(1 - 0.5774/X) \qquad (g) \qquad (38)$$

and when X = 4,

$$d_e = 0.31021\ L \qquad (mm)\ , \tag{39}$$

where L_o is now the length of a single bullet and L ($L = 2L_o$) is the geometric length of the combination.

Figure 9 depicts a downward view of a crystal of this type in the horizontal plane at an angle of 45° from the detector array. This angle presents the minimum possible shadow. Zero degrees, when either of the axes are parallel with the diode array, will give the shadow of the crystal's geometric length as in the case of the single column. Because of crystal symmetry, only the angles of 0 to 45° have to be considered.

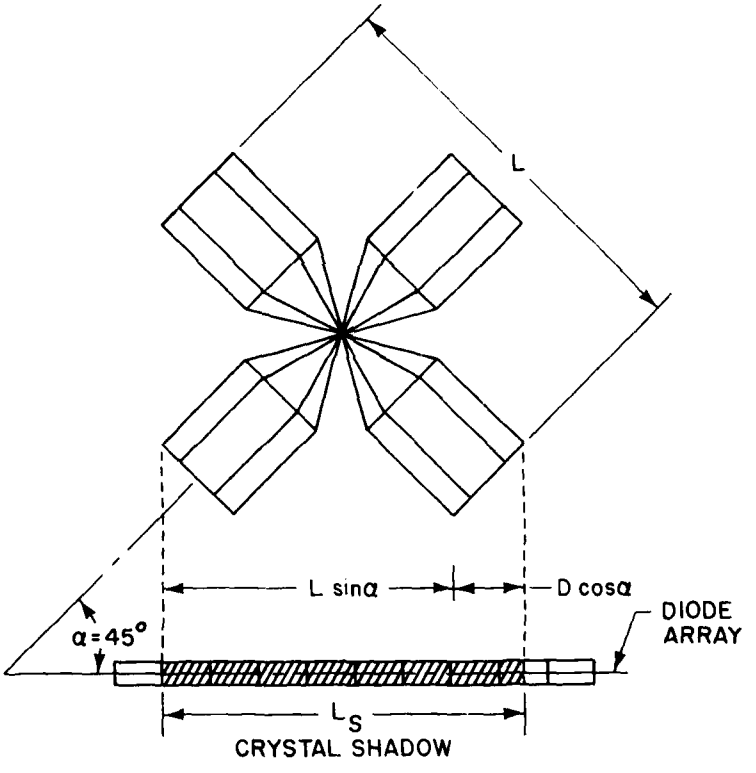

Figure 9. The Shadow Produced by a Combination of Four Bullets With a 45° Orientation from the Axis of the Diode Array as it Passes Through the Measuring Instrument

Since the outer appendages of this crystal are columnar in form, the shadow length can be expressed by the same equations as for the single columns (Eq. [16] and [17]). In this case, however, both α_H and α_V are the random angles from 0 to 45°.

The mean values from the 25 exponential distributions of Section 5 gave a γ_M of 0.34195 and a γ_Z of 0.33818 with a variance of -0.6 to 1.2 percent in γ_M and -0.9 to 1.5 percent in γ_Z. The variations in the values of the coefficients and exponents of the regression equations were also extremely small ranging from -1.8 to 2.8 percent for the coefficients and from -0.8 to 0.7 percent for the exponents. The mean exponent of 0.98409 very nearly matched the assumed 1.0 of the gamma method.

7. EXPERIMENTALLY DERIVED GEOMETRIC RELATIONSHIPS

As mentioned in Section 1, the assumed linear relationships of crystal length to diameter (D to T for plates) are in general agreement with experimentally derived equations.

Figure 10 is a plot showing the d_e's that result from using a linear geometric relationship for columns for crystal lengths of 0.025 to 0.5 mm compared to those determined from using the empirical equations of Auer and Veal[21] and Hobbs, et al.[22] Figures 11 and 12 are the same comparisons made for needles and hexagonal plates. The density of ice was assumed to be 0.0009 g mm^{-3} in all cases.

Since this study is concerned with the assessment of water content through the conversion of ice crystal measurements into terms of equivalent melted diameters, comparing d_e to crystal size is deemed more appropriate than the conventional plots of L vs D or D vs T. The solid lines in these figures delineate the results of using the linear relationships. The heavy lines depict the ratios used in this study, and the light lines show the differences that can be obtained with the indicated changes in geometric ratios.

In all three cases, the plots show that the results of the linear assumptions used herein compare favorably with those from the empirical equations for crystal sizes > 0.1 mm. The linear results are generally smaller for sizes < 0.1 mm, the exception being the case of needles where the d_e's from the experimentally derived equations vary considerably from one another and with the linear assumption. Caution must be used however, when making comparisons in the small cyrstal size range since the experimental data from which the empirical equations were derived were predominantly from larger sizes.

21. Auer, A.H. and Veal, D.L. (1970) The dimension of ice crystals in natural clouds, J. of Atmos. Sci. 27:919-926.

22. Hobbs, P.V., Chang S. and Locatelli, J.D. (1974) The dimensions and aggregation of ice crystals in natural clouds, J. Geo. Research 15:2199-2206.

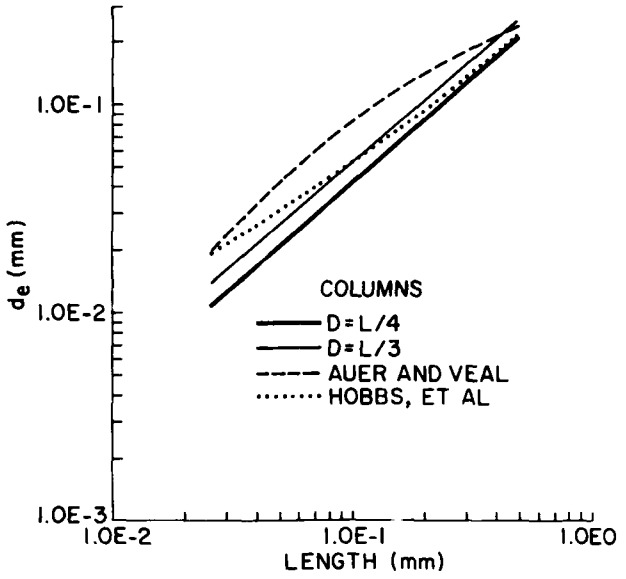

Figure 10. The d_e's Calculated for Columns Using Linear Geometric Relationships and those Derived from Experimental Data

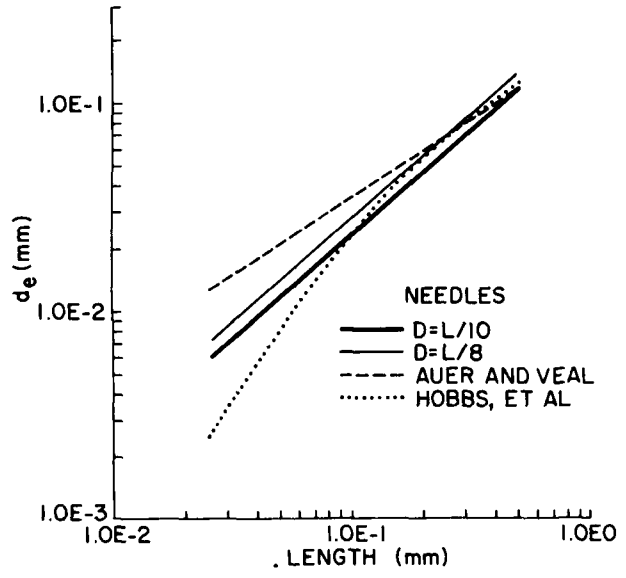

Figure 11. The d_e's Calculated for Needles Using Linear Geometric Relationships and those Derived from Experimental Data

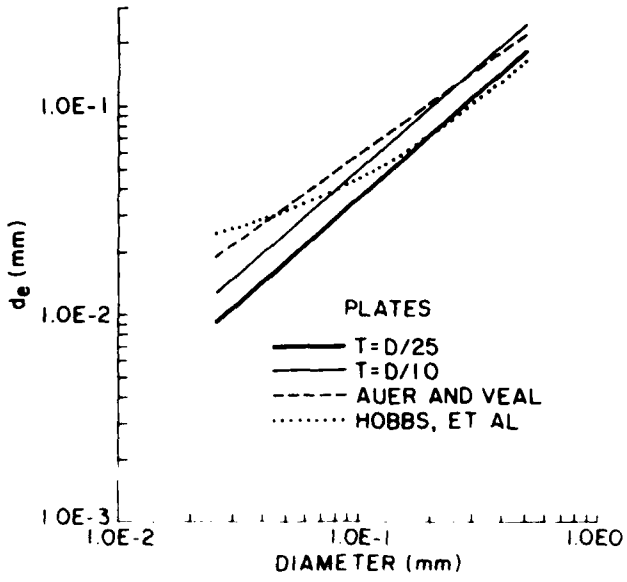

Figure 12. The d_e's Calculated for Hexagonal Plates Using Linear Geometric Relationships and those Derived from Experimental Data

Understandably, the actual experimental data exhibits considerable scatter which reflects the extreme difficulty in obtaining precise measurements and/or the diversity of the natural ice crystals that are being classified under specific category types. This is evidenced by the differences in the d_e's that result from use of the empirical equations from the two investigations presented in Figures 10 - 12. When comparisons of geometric relationships are made with other experimental investigations, such as presented in the paper of Hobbs, et al,[22] the differences in the findings of the various studies are more apparent. If each of these studies had the same degree of uncertainty in their measurements, the differences could only be associated with the actual physical structure of the crystals being sampled.

Any scenario in which airborne shadowgraph instrumentation is utilized for the purpose of determining atmospheric water content is almost certain to be a situation where little or nothing is known about the geometric relationships of the crystals in the immediate environment. In fact, the determination of a specific crystal type or mixture of types can sometimes be a problem. Therefore, general single crystal equations, ones that are able to approximate the crystal size to d_e relationships within specific category types, are necessary for the processing of aircraft acquired data.

In light of present knowledge, the conversion of aircraft-acquired measurements of single ice crystals (> 0.025 mm) into terms of liquid water (d_e) can be adequately described by logarithmic equations with a slope of 1.0 which result from linear geometric crystal size relationships. The ratios of linear assumptions can be altered for better agreement with any particular data set or group of data sets for any specified size range as shown in the plots. How well the determined mass of liquid water from a linear relationship agrees with an experimental finding is not only dependent upon the geometric assumption used but also on the shape of the crystal number density distribution. In general, the better the agreement in geometric relationships in the larger crystal sizes, the better the agreement in liquid water content since it is the larger crystals that contain the most mass.

If, for example, an idealized uniform distribution of columns composed of 20 classes over the size range of 0.025 to 0.5 mm is considered, use of the Auer and Veal equation will give a liquid water mass 102 percent larger than that of the linear D = L/4 relation used in this study whereas the result of the Hobbs equation is only 9 percent higher. The reason can be seen in Figure 10 where the dashed Auer and Veal curve lies completely above the heavy D = L/4 line while the dotted Hobbs curve is very close to the straight line at the larger crystal sizes. A change in the linear assumption to D = L/3 (light line in Figure 10) increases the linear-related mass determination so that the Auer and Veal result drops to just 13 percent above and Hobbs to 63 percent less than that from the linear. Figure 10 again shows the reason, where the dotted Hobbs curve crosses the light D = L/3 line at ~ 0.45 mm.

Different shape number density distributions will, of course, give varying results depending upon the distribution's slope. As the slope increases, the number of smaller particles increase as compared to the larger, thus the crystal size containing the most water content becomes progressively smaller.

If a situation occurs where it can be verified that the actual geometric relationship is in fact better described by a particular mathematical expression, that equation can be utilized with the concept of random orientation to determine the effects of crystal spatial positioning for any particular distribution. A gamma value will not be able to be derived since the development of this method is based on linear d_e - crystal size relationships.

8. SUMMARY OF RESULTS

Table 6 lists the mean values of γ_M and γ_Z for each of the crystal forms derived in Sections 5 and 6 and the minimum and maximum variations that resulted from those determined using the previously described five-situation format. The crystal types are arranged in ascending gammas which emphasize the effect that

Table 6. Summary of the Mean, Minimum, and Maximum Values of γ_M and γ_Z for the Crystal Configurations Determined in Sections 5 and 6

Crystal Form	Mean γ_M	Percentage From Mean Min	Max	Mean γ_Z	Percentage From Mean Min	Max
Hollow needles	0.24955	---	---	0.23019	---	---
Solid needles	0.31658	-2.0	4.0	0.29282	-2.5	4.4
Comb. of bullets	0.34195	-0.6	1.2	0.33818	-0.9	1.5
Hex plates	0.39058	-0.6	0.7	0.38528	-1.0	1.2
Solid bullets	0.45541	---	---	0.43330	---	---
Hollow cyl. columns	0.46342	-2.1	2.2	0.44103	-3.0	2.8
Solid hex columns	0.47979	---	---	0.45641	---	---
Solid cyl. columns	0.51106	-2.5	2.2	0.48625	-3.0	3.3

crystal density has on these values. Crystal symmetry shows a smaller effect in the uncertainties of the gamma values.

The uppermost gamma value that could be obtained would be from measurements of solid ice spheres. This hypothetical form would have perfect symmetry and the relationship with a spherical water drop would be

$$d_e = (\rho_I/\rho_\omega)^{1/3} D \qquad \text{(mm)} \qquad (40)$$

and since all L_S values would equal D both γ_M and γ_Z would equal the ratio of ρ_I/ρ_ω to the 1/3 power or 0.9655. The smallest conceivable gamma value would probably result from a hollow, thin-walled form having a very small density.

9. COMPARISON WITH OPERATIONAL PROCEDURE

The mass of liquid water contained in ice environments will continue to be derived from knowledge of crystal populations until some instrument is developed to make direct measurements. The accuracy of particle measuring devices such as the PMS 1-D are very important for the reliable determination of M. Equally important however, is how the physical measurements are converted into mass of equivalent liquid water. This process, which normally involves changing measured

ice particle parameters (length, L) into diameters (d_e) of equivalent spherical water drops, is commonly referred to as the "L to d" ("L_S to d_e" in this report) conversion.

The conversion equations that are an integral part in the processing of aircraft-acquired particle spectra at AFGL, have been derived from extensive literature evaluations and the personal observations and deductions of Dr. R. M. Cunningham while he was a member of the Meteorology Division.[23]

Table 7 lists the AFGL equations that would be most applicable to the basic crystal types that are considered in this study. Also included, are the corresponding γ_M relationships that were derived in this investigation.

Table 7. The Conversion Equations Currently Being Used at AFGL and the Theoretically Derived Equations for the Comparable Crystal Types Considered in this Study

AFGL Type	AFGL Eqs.	Derived γ_M Crystal Eqs.
Columns	$d_e = 0.438\ L_S^{1.0}$	$d_e = 0.47970\ L_S$
Needles	$d_e = 0.256\ L_S^{0.670}$	$d_e = 0.31658\ L_S$
Plate Family	$d_e = 0.340\ L_S^{0.783}$ (<1 mm)	$d_e = 0.39058\ L_S$
	$d_e = 0.340\ L_S^{0.685}$ (>1 mm)	
Bullet-Rosettes	$d_e = 0.256\ L_S^{0.667}$ (<0.2 mm)	$d_e = 0.34195\ L_S$
	$d_e = 0.438\ L_S^{1.0}$ (>0.2 mm)	

Some interesting ponderable points are evident when considering the AFGL equations listed in this table. All equations are of power function form and the same equation, which has a slope of 1.0, is applicable to columns and bullet-rosettes with sizes larger than 0.2 mm. Note the similarity between this equation and Eq. (8). Also, the equation for bullet-rosettes with sizes less than 0.2 mm and the one for needles are nearly identical.

Figure 13 shows the different relationships of d_e with L_S for the four types designated in Table 7 with measured particle sizes of 0.025 to 0.5 mm. The curves from the gamma equations are derived using γ_M since it is the determination of M

23. Cunningham, R. M. (1978) Analysis of particle spectral data from optical array (PMS) 1-D and 2-D sensors, Preprints Fourth Symposium on Meteorological Observations and Instrumentation, Denver, Colorado, 10-14 April 1978, 345-350.

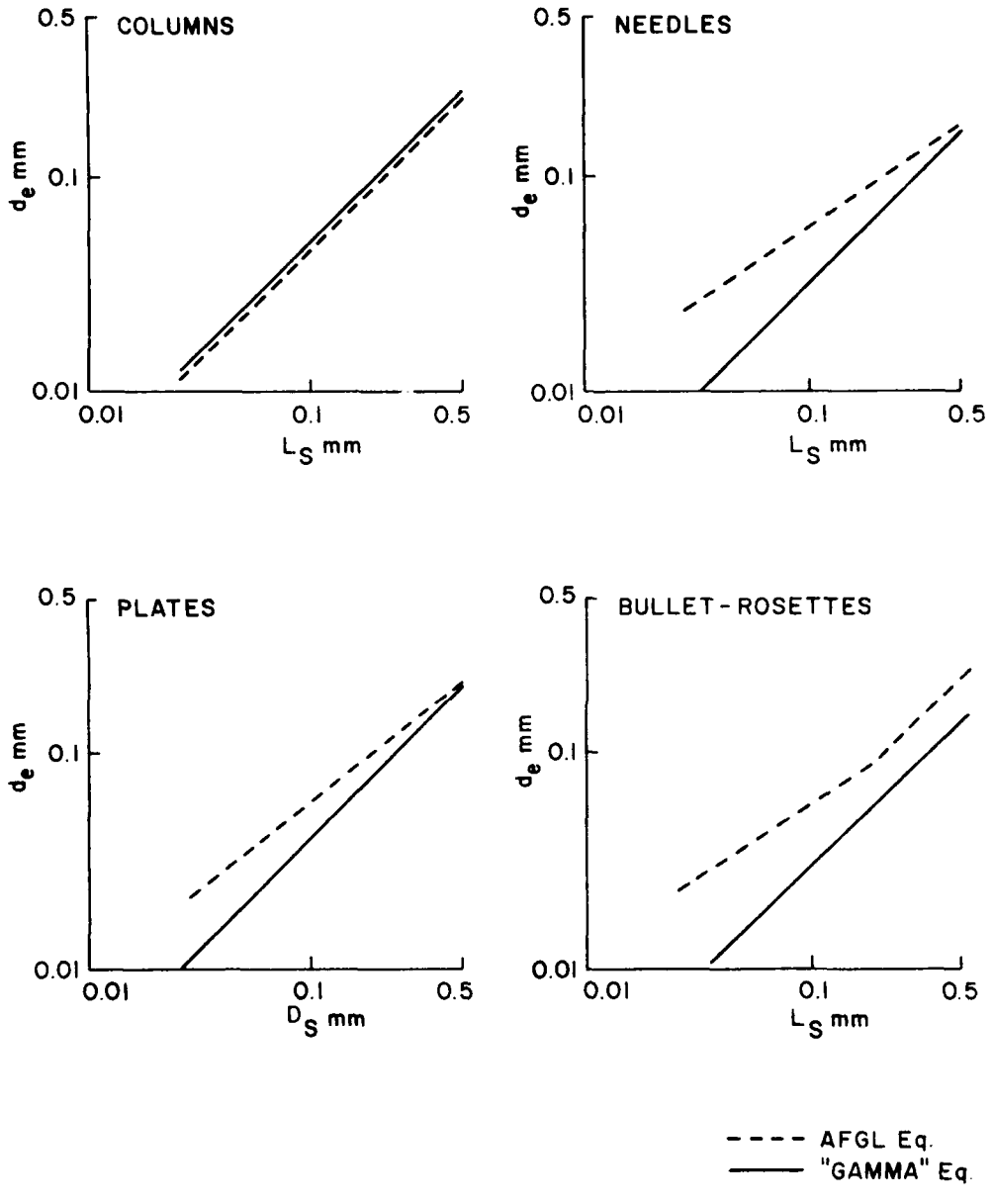

Figure 13. Comparison of the AFGL "L_S to d_e" Conversion Equations with those Derived Using the Gamma Method

that is of primary importance. The two column curves are offset reflecting the difference in the multiplication factors and could be the effect of assumed crystal density (D to L ratio) and/or column orientation. The curve for bullet-rosettes is above the gamma curve and diverges below 0.2 mm but becomes parallel above 0.2 mm because of the two equation AFGL conversion. The curves for needles and plates show a drastic divergence with smaller L_S sizes.

The AFGL equations are for crystal environments containing specific types and are not designated for single crystals only, as in the case of the relations derived in this study. The application of the general conversion equations to a single crystal environment could result in appreciable error in the assessment of M. Deviation from true M will vary considerably with crystal type, size, number density, and shape of distribution. One means of obtaining some information as to the possible uncertainties is to apply the conversion equations to a number density having a known mass. One distribution for each crystal type was chosen from the $\Lambda = 25$ test situations described in Table 3. One for each type was also taken from the $\Lambda = 10$ case. The M's for those number densities were calculated using the AFGL and γ_M equations from Table 7 and compared to the actual M. These results are listed in Table 8.

Table 8. Percentage Difference ($\Delta M/M_T$) for the Four Crystal Types Calculated from the AFGL Equations and Average γ_M's for Two Different Distributions

	Percentage $\Delta M/M_T$			
	Using $\bar{\gamma}_M$		Using AFGL Eq.	
AFGL Type	$\Lambda = 25$	$\Lambda = 10$	$\Lambda = 25$	$\Lambda = 10$
Columns	2.1	-3.7	-22.2	-26.7
Needles	2.9	1.1	533.6	144.6
Plate Family	2.8	-0.5	204.8	60.3
Bullet-Rosettes	2.4	1.2	359.1	137.7

It is evident from both Figure 13 and the results in Table 8 that the column type will be the only one that will give a predictable deviation for any distribution since the two equations differ by a factor of 1.095. The other three classifications vary considerably from one situation to another.

10. CONCLUSIONS

The determination of the mass of liquid water from ice hydrometeor environments is severely handicapped by the absence of an operational device that can directly and reliably record such information. The result of this technological void is that mass has to be derived from knowledge of crystal populations that are ascertained with instruments such as the PMS 1-D. The accuracy of any device used in the sizing and counting of particles is, of course, important for the correct assessment of M but so is the manner in which the measured ice crystal parameters are converted into diameters of equivalent water drops.

The study presented in this report is an evaluation of this conversion problem through the analyses of assumed single crystal environments. Admittedly, these assumed situations are not nearly as complex as those presented to a sampling aircraft but they have served a useful purpose by providing some definitive conclusions along with some suggestions for possible future investigations.

Foremost is the demonstrated feasibility of simulating ice particle measurements by mathematical modeling with the use of a computer. The complexity of an assumed situation and how well it compares to reality is limited only by the scope of the investigation and the knowledge and ability of the investigator. For instance, if the requirement presents itself, slight programming changes in the model used in this report would allow the analysis of mixed-type, single crystal situations. A more ambitious study could explore the effect on the measuring and conversion processes on multicrystal structures. In such case, a computer could be used to generate random points for crystal attachment and thus simulate an aggregation process by making assumptions about the approximate shapes and densities of the aggregates.

This study also indicates that a number density distribution constructed from the measurements of a shadowgraph instrument could, because of crystal orientation, be a false representation of the actual crystal environment. The analysis of the uniform column distribution (Section 4, Figure 5) show that crystal configurations having elongated forms (columns, bullets, needles) can result in measured distributions with more smaller and less larger particles than that of the true environment. Random orientation, however, has little effect on the number density distributions of crystals having more proportional configurations (plates for example).

Another conclusion brought forth by this study is that the use of a power function relationship (other than a slope of 1.0) for converting L_S to d_e could result in considerable error if the measurements were made on single crystals. As particles join to form aggregates, the number of air spaces in the lattice should increase with increasing aggregate size for most situations (bundles of needles would be an

exception). Thus, the aggregate density most probably decreases with increasing size. Apparently, some type of variable relationship exists between the various aggregate sizes and their corresponding d_e's.

This investigation points toward a logarithmic relationship with a slope of 1.0 as best for single crystals. Logic dictates that some slope less than 1.0 would be applicable for different size aggregates. If these arguments have any validity, then something other than a straight-line logarithmic format has to be used to define the L_S to d_e relationships that exist throughout the complete growth process from single crystal on through the varying stages of aggregation.

References

1. Barnes, A.A., Nelson, L.D., and Metcalf, J.I. (1974) Weather documentation at Kwajalein Missile Range, 6th Conference on Aerospace and Aeronautical Meteorology, American Meteorological Society, 66-69, Air Force Surveys in Geophysics, No. 292, AFCRL-TR-74-0430, AD A000 925, 14 pp.
2. Barnes, A.A., Metcalf, J.I., and Nelson, L.D. (1974) Aircraft and radar weather data analysis for PVM-5, Air Force Surveys in Geophysics, No. 297, AFCRL/Minuteman Report No. 1. AFCRL-74-0627, AD B004 290, 47 pp.
3. Plank, V.G. (1974) Liquid-water-content and hydrometeor size-distribution information for the SAMS Missile Flights of the 1971-72 season at Wallops Island, Virginia, Special Reports, No. 178, AFCRL/SAMS Report No. 3, AFCRL-TR-74-0296, AD A002 370, 143 pp.
4. Plank, V.G. (1977) Hydrometeor data and analytical-theoretical investigations pertaining to the SAMS Missile Flights of the 1972-73 season at Wallops Island, Virginia, Environmental Research Papers, No. 603, AFGL/SAMS Report No. 5, AFGL-TR-77-0149, AD A051 192, 239 pp.
5. Varley, D.J. (1980) Microphysical Properties of Large Scale Cloud Systems, 1-3 March 1978, Environmental Research Papers, No. 690, AFGL-TR-80-0002, AD A083 140, 100 pp.
6. Cohen, I.D. (1981) Development of a Large Scale Cloud System, 23-27 March 1978, Environmental Research Papers, No. 739, AFGL-TR-81-0127, AD
7. Varley, D.J. (1978a) Cirrus Particle Distribution Study, Part 1, Air Force Surveys in Geophysics, No. 394, AFGL-78-0192, AD 061 485, 71 pp.
8. Varley, D.J. and Brooks, D.M. (1978) Cirrus Particle Distribution Study, Part 2, Air Force Surveys in Geophysics No. 411, AFGL-TR-78-0248, AD A063 807, 108 pp.
9. Varley, D.J. (1978b) Cirrus Particle Distribution Study, Part 3, Air Force Surveys in Geophysics No. 404, AFGL-TR-78-0305, AD 066 975, 67 pp.

10. Varley, D.J. and Barnes, A.A. (1979) Cirrus Particle Distribution Study, Part 4, Air Force Surveys in Geophysics No. 413, AFGL-TR-79-0134, AD 074 763, 91 pp.

11. Cohen, I.D. (1979) Cirrus Particle Distribution Study, Part 5, Air Force Surveys in Geophysics, No. 414, AFGL-TR-79-0155, AD A077 361, 81 pp.

12. Cohen, I.D. and Barnes, A.A. (1980) Cirrus Particle Distribution Study, Part 6, Air Force Surveys in Geophysics, No. 430, AFGL-TR-80-261, AD A096 772, 106 pp.

13. Varley, D.J., Cohen, I.D. and Barnes, A.A. (1980) Cirrus Particle Distribution Study, Part 7, Air Force Survey in Geophysics, No. 433, AFGL-TR-80-0324, AD A100 269, 82 pp.

14. Church, J.F., Pocs, K.K., and Spatola, A.A. (1975) The continuous aluminum foil sampler; design operation, data analysis procedures, and operating instructions, Instrumentation Papers, No. 235, AFCRL-TR-75-0370, AD A019 630, 70 pp.

15. Knight, C.A., Knight, N.C., Grotewold, W.W. and Cannon, T.W. (1977) Interpretation of foil impactor impressions of water and ice particles. J. Appl. Met. 16:997-1002.

16. MacCready, P.D. and Todd, C.J. (1964) A continuous particle Sampler, J. Appl. Met. 3:450-460.

17. Hallett, J. (1976) Measurement of Size Concentration and Structure of Atmospheric Particulates by the Airborne Continuous Particle Replicator, Final Report, AFGL-TR-76-0149, AD A033 067, 92 pp.

18. Knollenberg, R.G. (1970) The optical array: an alternative to scattering or extinction for airborne particle size determination, J. Appl. Meteor. 1:86-103.

19. Crane, R.K. (1978) Evaluation of Uncertainties in the Estimation of Hydrometeors Mass Concentrations using Spandar Data and Aircraft Measurements, Scientific Report No. 1, AFGL-TR-78-0118, AD A059 223, 107 pp.

20. Magone, C. and Lee, C.W. (1966) Meteorological classification of natural snow crystals, J. of the Faculty of Science, Hokkaido University, Ser. VII (Geophysics) 4:321-335.

21. Auer, A.H. and Veal, D.L. (1970) The dimension of ice crystals in natural clouds, J. of Atmos. Sci. 27:919-926.

22. Hobbs, P.V., Chang S. and Locatelli, J.D. (1974) The dimensions and aggregation of ice crystals in natural clouds, J. Geo. Research 15:2199-2206.

23. Cunningham, R.M. (1978) Analysis of particle spectral data from optical array (PMS) 1-D and 2-D sensors, Preprints Fourth Symposium on Meteorological Observations and Instrumentation, Denver, Colorado, 10-14 April 1978, 345-350.

List of Symbols

d	Diameter of a spherical water drop
d_e	Equivalent diameter of a spherical water drop
d_{e_i}	Midclass, equivalent melted diameter of an ice crystal of the "i" class
D	Diameter of an ice crystal
L	Length of an ice crystal
L_S	Length of shadow produced by an ice crystal passing through an electrooptical measuring device
m	Mass of an ice crystal
M	Mass of liquid water
M_T	True mass of liquid water contained in a specific ice crystal environment
N_i	Number of particles in "i" class
N_o	The zero intercept of an exponential distribution function
T	Thickness of a hexagonal plate
X	Ratio of diameter to length of a cylindrical ice crystal or thickness to diameter for plates
X_1	Ratio of inner diameter of a hollow column to crystal length
Z	Radar-reflectivity factor

Z_T	True radar-reflectivity factor calculated from a specific ice crystal environment
α	Crystal orientation angle in degrees
α_H	Crystal orientation angle in the horizontal plane
α_V	Crystal orientation angle in the vertical plane
γ	Coefficient of the measured length to equivalent melted diameter conversion equation
γ_M	Factor used for the calculation of M in the "gamma" method
γ_Z	Factor used for the calculation of Z in the "gamma" method
Λ	Exponential "slope factor" in the distribution function for the number concentration of the particles
ϕ	Exponent of the measured length to equivalent melted diameter conversion equation
ρ_I	Density of ice
ρ_ω	Density of water